Appl. Phys. B 68, 1047–1054 (1999) / DOI 10.1007/s003409901500

Applied Physics B
Lasers
and Optics

Differentiation and subtraction of amplitude and phase images using a photorefractive novelty filter

M. Sedlatschek, J. Trumpfheller, J. Hartmann, M. Müller, C. Denz, T. Tschudi

Technische Universität Darmstadt, Institut für Angewandte Physik, Hochschulstraße 6, D-64289 Darmstadt, Germany
(Fax: +49-6151/16-4123, E-mail: Cornelia.Denz@physik.tu-darmstadt.de)

Received: 14 November 1998/Revised version: 18 January 1999/Published online: 12 April 1999

Abstract. In this article, we demonstrate the capability of a two-beam coupling photorefractive optical novelty filter of detecting changes in the amplitude or phase of optical images. These changes may either be continuous or discrete in time. The performance of the two-beam coupling novelty filter is investigated and expressions for the output contrast corresponding to phase and amplitude changes based on a novel, simple interference model of two-beam coupling are derived. These expressions are verified by experimental results on the novelty contrast, revealing that the amplitude contrast is not described correctly by the commonly accepted coupled-wave theory. The novelty filter was applied to the detection of temporally continuous phase changes provided by a gas flow and moving microscopic objects. A novel scheme for image subtraction is also demonstrated, showing the novelty filter's ability to detect temporally discrete changes.

PACS: 42.65 H; 42.30; 07.07.D

Due to its inherent parallelism, optics is considered advantageous for processing high-resolution images. For temporally changing images, a key processing element is the so-called optical novelty filter [1]. An optical novelty filter is a device that detects temporal changes in an image sequence and suppresses its stationary parts. Applications of optical novelty filters include, for example, object tracking [2, 3], motion detecting microscopy [4], edge enhancement [5, 6], visualization of plasma jets [7], novelty-filtering intensity correlation [8], audio sound processing [13] and phase front measurement [10, 11]. Most optical novelty filters realized up to now are based on the photorefractive effect. However, configurations based on the same principle but other nonlinear optical effects such as phase conjugation in an organic film [12] or using photon-echo [9] do exist. The novelty filter based on photorefractive two-beam coupling used in this work was first proposed and demonstrated by Cronin-Golomb et al. [14]. This novelty filter configuration exhibits two main advantages – a high contrast and the relative ease of adjustment.

Dedicated to Prof. Dr. Eckard Krätzig on the occassion of his 60th birthday.

Despite the number of publications on photorefractive novelty filters, a rigorous treatment of its main figure of merit, the novelty contrast, that is in agreement with experiments, is still lacking. We show, that the predictions of the commonly used coupled-wave theory (see, for example, [15]) are not in agreement with experimental results. We therefore develop a simple theoretical model of the two-beam coupling novelty filter that is based on the simple mechanisms of diffraction and interference and is confirmed by experimental results. We then show that, following from the working principle of the novelty filter, it can be operated in two modes, image differentiation and image subtraction. We then report on experimental realizations of different applications of the photorefractive two-beam coupling novelty filter. The device was applied to the visualization of a gas flow and motions of biological objects in a novelty filtering microscope. We have also realized an optical object inspection system that is based on the subtraction of subsequent images.

1 Interference model of photorefractive two-beam coupling

The working principle of the two-beam coupling photorefractive novelty filter has already been described by Anderson and Feinberg [1]. Novelty filtering is performed by the destructive interference of a current input image and the readout of an image holographically stored in the photorefractive index grating. Due to the dynamic nature of the photorefractive grating formation, the latter is an exponential time average of all previous input images. Based on this working principle, we now develop a new and simple model of photorefractive two-beam coupling based on interference and compare its predictions of the novelty filter contrast to the predictions of the widely accepted coupled-wave theory as well as with experiments.

The idea of our model is visualized in Fig. 1. Beams 1 and 2 are incident on the crystal and form an interference grating I (dashed lines) with grating period Λ, relative to which both beams have an angle θ. Without loss of generality, we assume the grating vector to be parallel to the c axis.

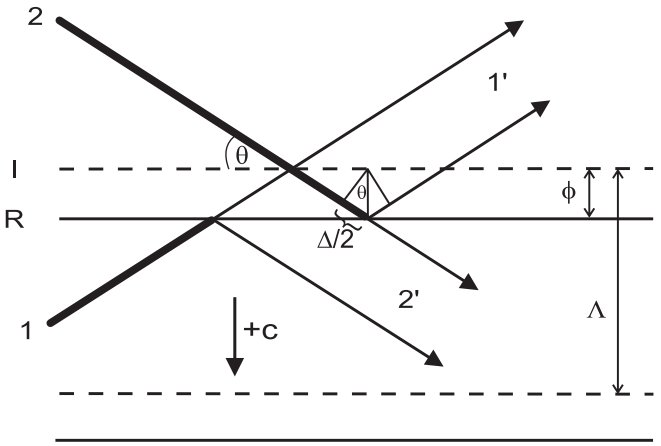

Fig. 1. Interference model of photorefractive two-beam coupling. Beams 1 and 2 form an interference grating I (*dashed lines*) with grating wavelength Λ, that creates a refractive index grating R (*solid lines*), shifted by a phase of ϕ relative to the interference grating. Consequently, the transmitted part of beam 1 (2) interferes with the diffracted part of beam 2 (1)

A refractive index grating R (solid lines) is created via the photorefractive effect, which is spatially shifted with respect to interference grating. In purely diffusion-dominated crystals, this grating phase shift is exactly $\pi/2$, but can deviate from this value even in $BaTiO_3$ crystals [16, 17]. Therefore, the grating phase shift is referred to as ϕ in this article.

Beams 1 and 2 are diffracted by the refractive index grating they have produced with diffraction efficiency η at output port $1'$ ($2'$), the diffracted part of beam 2 (1) interferes with the transmitted part of beam 1 (2). The energy transfer in photorefractive two-beam coupling originates from the different phase shifts of the interference in the two ports. When diffracted from a phase grating, the first order of diffraction has a relative phase shift of $\pi/2$ with respect to the zero-order (i.e. transmitted) beam [18, 19]. In addition, the diffracted part of beam 2, then propagating in the direction of beam 1, experiences an additional phase shift because it is diffracted from the index grating which is spatially shifted with respect to the interference grating and thus has to propagate over an additional path length of Δ (see Fig. 1). This additional path length can easily be shown to be equivalent to the grating phase shift ϕ, independent of the angle of incidence θ, as long as the phase shift itself is independent of θ. This situation holds for the case of diffusion-dominated crystals ($\phi \approx 90°$), which is the case considered in this article. The path difference and thus the phase shift have the opposite sign for the diffracted part of beam 1 with respect to beam 2. Thus, incorporating the phase shift $\pi/2$ due to diffraction from a phase grating, which always has positive sign, the two beams experience the following total phase shifts φ:

$$\text{diffracted part of beam 1:} \quad \varphi_{\mathrm{d}1} = \frac{\pi}{2} - \phi\,,$$
$$\text{diffracted part of beam 2:} \quad \varphi_{\mathrm{d}2} = \frac{\pi}{2} + \phi\,. \tag{1}$$

Consequently, we have destructive interference of the transmitted portion of beam 1 and the diffracted portion of beam 2 in output port $1'$ and constructive interference of the transmitted portion of beam 2 and the diffracted portion of beam 1 in output port $2'$. Thus, beam 2 is amplified and beam 1 is depleted. When an image is imposed on beam 1, novelty filtering is performed, whereas coherent image amplification occurs when the image is imposed on beam 2.

Let us now calculate the intensities of the two beams at the output ports $I_1(L) = I_1'$ and $I_2(L) = I_2'$ (with interaction length L of the beams) as functions of the input intensities $I_1(0)$ and $I_2(0)$ according to the interference model. It is well known that the intensity of two interfering collinear waves of intensities I_1 and I_2 with phase difference Ψ is given by

$$I = |E_1 + E_2|^2 = I_1 + I_2 + 2\sqrt{I_1 I_2}\cos\Psi\,. \tag{2}$$

To calculate the intensities at the output ports, we first have to determine the expressions for the two waves that interfere there. It is assumed that a portion $I_{1,2}^{\mathrm{d}} = \eta I_{1,2}$ of every wave is diffracted into the direction of the other and a portion $I_{1,2}^{\mathrm{t}} = (1-\eta) I_{1,2}$ is transmitted, where η is the effective diffraction efficiency of the refractive index grating. Using (2), the output intensities become:

Output port $1'$:

$$\begin{aligned} I_1' &= I_1^{\mathrm{t}} + I_2^{\mathrm{d}} + 2\sqrt{I_1^{\mathrm{t}} I_2^{\mathrm{d}}}\cos\varphi_{\mathrm{d}2} \\ &= (1-\eta) I_1 + \eta I_2 + 2\sqrt{(1-\eta)I_1 \eta I_2}\cos\varphi_{\mathrm{d}2}\,. \end{aligned} \tag{3}$$

Output port $2'$:

$$\begin{aligned} I_2' &= I_2^{\mathrm{t}} + I_1^{\mathrm{d}} + 2\sqrt{I_2^{\mathrm{t}} I_1^{\mathrm{d}}}\cos\varphi_{\mathrm{d}1} \\ &= (1-\eta) I_2 + \eta I_1 + 2\sqrt{(1-\eta)I_2 \eta I_1}\cos\varphi_{\mathrm{d}1}\,. \end{aligned} \tag{4}$$

All parameter dependencies of photorefractive two-beam coupling are contained in the diffraction efficiency.

The diffraction efficiency of a photorefractive index grating with arbitrary phase shift ϕ was first derived by Kukhtarev et al. [20]. Assuming hole-conducting $BaTiO_3$, it can be written as

$$\eta_{\mathrm{kuk}} = \frac{2m\exp(-\gamma L/2)\left[\cosh(-\gamma L/2) - \cos\left(\frac{\gamma L}{2\tan\phi}\right)\right]}{(1+m)\left[1+m\exp(-\gamma L)\right]}\,. \tag{5}$$

Here, γ is the photorefractive coupling coefficient given by $\gamma = 2\pi n_1 \sin\phi/(\lambda\cos\theta)$, where θ is the half-angle of intersection of the two beams, and n_1 describes the modulation depth of the photorefractive index grating. m is the intensity ratio of the incoming beams, defined as $m = I_1(0)/I_2(0)$.

The diffraction efficiency of (5) accounts for the diffraction in all directions. For photorefractive beam coupling described by the interference model, only the portion of the diffracted beam collinear to the transmitted part of the other beam is relevant. Due to the effect of hologram bending for $\phi \neq \pi/2$ [20], diffraction also occurs in other directions in this case, thus not contributing to the beam coupling. The diffraction efficiency relevant to the beam coupling is thus different from η. The hologram bending increases with increasing deviation of the grating phase shift ϕ from $\pi/2$, thus the effective diffraction efficiency must decrease when ϕ approaches 0. In the case of $\phi = \pi/2$, no hologram bending occurs and the effective diffraction efficiency is equal to the one given in (5). For $\phi = 0$, the hologram is only tilted and the Bragg-diffracted beam thus has no component collinear to the other writing beam, requiring $\eta = 0$ in our model. Our simple interference model gives no information about the diffraction efficiency. Thus, we have to find an expression that leads

to results in agreement with experiments. A good choice is multiplying Kukhtarev's expression for the diffraction efficiency by a factor of $\sin\phi$, which fulfills the requirements for η mentioned above. The diffraction efficiency relevant for beam coupling thus reads

$$\eta \to \eta_{\mathrm{kuk}} \sin\phi = \frac{2m\exp(-\gamma L/2)\left[\cosh(-\gamma L/2) - \cos\left(\frac{\gamma L}{2\tan\phi}\right)\right]}{(1+m)\left[1+m\exp(-\gamma L)\right]} \sin\phi \,. \quad (6)$$

Coherent signal amplification is known to be described excellently by the coupled wave theory. Having chosen the effective diffraction efficiency η as above, the signal gain,

$$g = \frac{I_2(L)}{I_2(0)} = (1-\eta) + \eta m + 2\sqrt{(1-\eta)\eta m}\cos\varphi_{\mathrm{d1}} \,, \quad (7)$$

agrees with the signal gain due to the coupled wave theory with a deviation of less than 2% for typical experimental values of $10^{-4} < m < 10^4$ and $\gamma L \approx 3-4$ for $\phi \neq \pi/2$. For example, a value of $\phi = 70°$ and $m = 10^4$ leads to a deviation of 1%, a value of $\phi = 87°$ and the same m in a deviation of less than 0.2%. For $\phi = \pi/2$, i.e. a purely diffusion-dominated crystal, a complete agreement of the gain due to the interference model using this effective diffraction efficiency with the gain due to the coupled-wave theory is obtained, which can also be proved analytically [21]. This justifies the choice of η according to (6).

2 Contrast for amplitude and phase changes

The most important figure of merit for an optical novelty filter is the visibility of the novel parts in an image compared with the unchanged parts. This leads to a definition of the novelty contrast as the intensity ratio of the novel part of the image to the same part when it is no novelty [1, 22]. When amplitude changes are considered, the change can be defined by switching on or off a complete image bearing beam (beam 1 in our nomenclature). The alternating switching on and off of the image bearing beam then leads to a series of peaks with exponential decay [22]. The appearance of a novelty thus corresponds to switching on beam 1 without a grating in the crystal, and consequently the ouptut intensity $I_1(0)$. When the novelty filter has adapted to the change, a grating is formed due to the interaction with beam 2 and the output intensity of the depleted image beam is thus $I_1(L)$. The amplitude contrast C_{a} is thus written as

$$C_{\mathrm{a}} = \frac{I_1(0)}{I_1(L)} \,. \quad (8)$$

Because coupled-wave theory (see, for example, [15]) is known to describe coherent signal amplification very well, it was also the theory of choice in previous publications for the description of the novelty filter contrast [1, 4]. According to the coupled-wave theory, the contrast for amplitude changes is

$$C_{\mathrm{a}} = \frac{I_1(0)}{I_1(L)} = \frac{1+m^{-1}\exp(\gamma L)}{1+m^{-1}} \,. \quad (9)$$

Experiments for the investigation of the novelty contrast have been performed with the relatively simple setup shown in Fig. 2. Experimental values of the amplitude contrast for the two-beam coupling photorefractive novelty filter were obtained using a nominally undoped, single-domain $BaTiO_3$ crystal ($6.4 \times 2.4 \times 3.2$ mm) in a configuration using extraordinary polarization to exploit the large electrooptic r_{42} coefficient and are shown in Fig. 3. The incident angles on the crystal are 83° and 53° with respect to the normal of the crystal surface for the reference and signal beam, respectively (compare Fig. 2). The figure also shows theoretical curves according to the coupled-wave theory (9) for different realistic values of the coupling parameter γL. It is evident that the experimental values are not reproduced by theoretical curves according to the coupled-wave theory. For example, it is shown easily by differentiation, that (9) never has a maximum. However, it turns out that the simple interference model developed above can be used to describe the experimental results for the ampliude contrast. According to the interference model, the

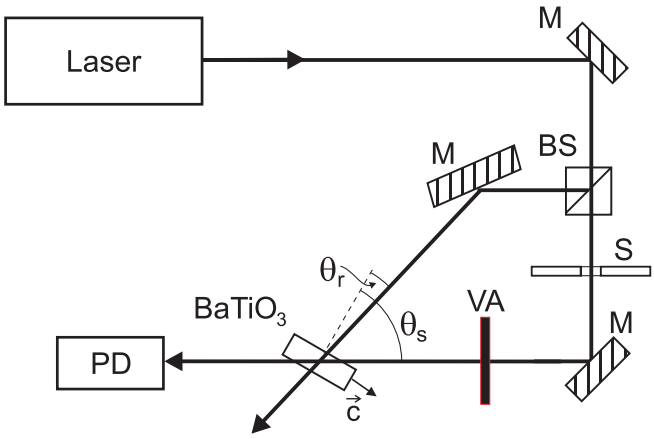

Fig. 2. Experimental setup for the investigation of the novelty contrast. M: mirrors, BS: beam splitter, VA: variable attenuator, S: shutter, PD: photo diode

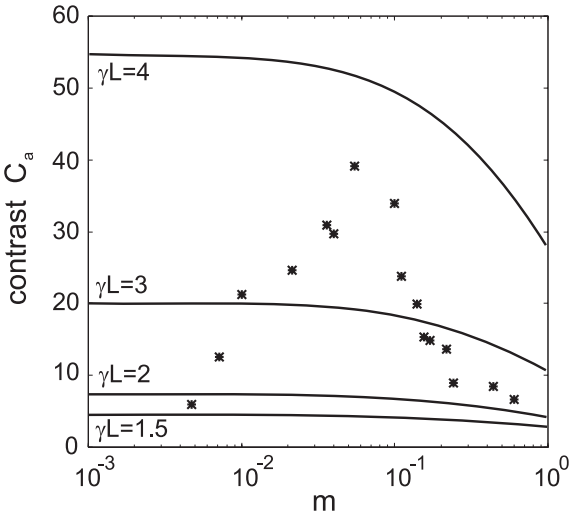

Fig. 3. Experimentally obtained amplitude contrast C_{a} as a function of the intensity ratio m using an undoped $BaTiO_3$ crystal (*stars*) and theoretical curves according to the coupled-wave theory (9) for $\gamma L = 1.5, 2, 3, 4$

amplitude contrast is

$$C_{\mathrm{a}} = \frac{I_1(0)}{I_1(L)} = \left[\, 1-\eta+\frac{\eta}{m}+\, 2\sqrt{\frac{\eta}{m}(1-\eta)}\cos\varphi_{\mathrm{d2}} \,\right]^{-1} , \tag{10}$$

where we have used $I_2(0) = I_1(0)/m$. The diffraction efficiency is given by (6). For $\phi = \pi/2$, we again obtain complete agreement with coupled-wave theory, which also implies that no maximum occurs in the curve. However, for $\phi \neq \pi/2$, considerable deviations compared to the coupled-wave theory occur. The contrast according to (10) can be shown to increase when φ_{d2} approaches π, which means that ϕ approaches $\pi/2$ and with increasing γL. The first requirement is fulfilled when the charge transport in the photorefractive medium is pure diffusion and the second evidently corresponds to strong beam coupling.

Taking these theoretical results into account, we were able to increase the amplitude contrast by a factor of 10. Using a cobalt-doped $BaTiO_3$ crystal ($8.5 \times 3.6 \times 5.5$ mm) under the same conditions as for the nominally undoped $BaTiO_3$, a contrast larger than 400 was achieved. In Fig. 4, these experimental results are plotted together with a fit of the interference model according to the optimal contrast condition in (10) for the fit parameters $\gamma L = 8.8$ and $\phi = 85°$, showing good agreement between the experimental data and the interference model. Using this theory and the appropriate fit parameters, the experimental data of Fig. 3 could also be found to be in good agreement with the theoretical behaviour.

Large beam coupling as in this case of high contrast is necessarily connected with strong beam fanning, which contributes to depletion of the image-bearing beam and alters the beam intensity ratio in the interaction region. Thus, we have included a correction factor of 0.125 in the intensity ratio m, accounting for this effect. In our fit parameters, a deviation of the grating phase shift ϕ from the commonly assumed value of 90° occurs. Such a deviation has already been measured using different methods in several samples of $BaTiO_3$ (see, for example, [16, 17]).

The phase contrast C_{p} as the novelty filter's response to phase changes is calculated in the same manner as for the amplitude contrast. It is given by the intensity ratio of the novelty filter output with and without a phase change of $\Delta\psi$

$$C_{\mathrm{p}}(\Delta\psi) = \frac{I_1(L,\Delta\psi)}{I_1(L,\Delta\psi=0)} = \frac{1-\eta+\frac{\eta}{m}+\, 2\sqrt{\frac{\eta}{m}(1-\eta)}\cos(\varphi_{\mathrm{d2}}+\Delta\psi)}{1-\eta+\frac{\eta}{m}+2\sqrt{\frac{\eta}{m}(1-\eta)}\cos\varphi_{\mathrm{d2}}} . \tag{11}$$

The diffraction efficiency is given by (6) as for the amplitude contrast. A slight deviation of φ_{d2} from π has no noticeable effect on the phase contrast according to (11) and thus we assume $\varphi_{\mathrm{d2}} = \pi$. Then, using the replacement

$$v = \frac{2\sqrt{\frac{m}{\eta}-1}}{\frac{m}{\eta}-2\sqrt{\frac{m}{\eta}-1}} , \tag{12}$$

(11) can be written in the simple form:

$$C_{\mathrm{p}} = 1 + v(1-\cos\Delta\psi) , \tag{13}$$

which has already been derived in a different way for the beam-fanning novelty filter [10]. Experiments for measuring the phase contrast have been performed using a liquid-crystal phase modulator to introduce phase shifts. In Fig. 5, experimental values of the phase contrast are shown together with a fit of (11). The only fit parameter γL was estimated as $\gamma L = 1.54$, showing a good agreement between theory and experiment.

3 Continuous changes: gas flows and microscopic objects

Soon after its discovery, it was recognized that a photorefractive optical novelty filter performs a temporal differentiation of the incoming optical information [1, 14]. Due to the continuous erasing and re-writing of the photorefractive hologram formed in the crystal, it represents the time-exponential average of the past images. Due to the destructive interference,

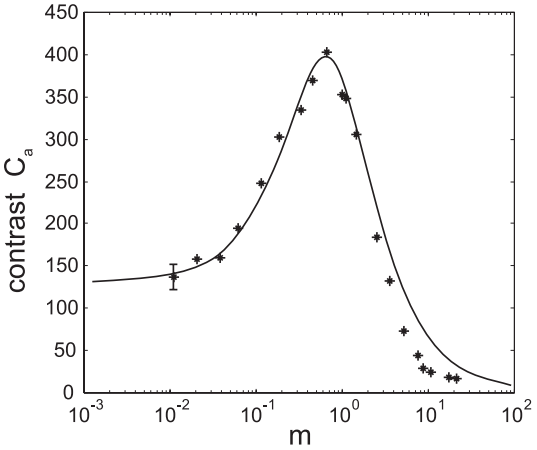

Fig. 4. Amplitude contrast C_{a} as a function of the intensity ratio m using a cobalt-doped $BaTiO_3$ crystal (stars). The solid curve is a fit of the interference model (10) with parameters $\gamma L = 8.8$, $\phi = 85°$, and correction factor 0.125 for the intensity ratio m

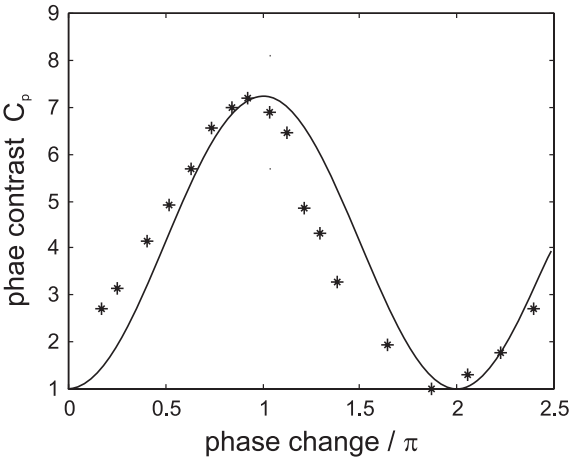

Fig. 5. Dependence of phase contrast C_{p} on the magnitude $\Delta\psi$ of the phase change. Experimental values (*stars*) and fit of the theoretical curve with fit parameter $\gamma L = 1.54$

which is the working principle of the novelty filter as discussed in Sect. 1, this time-averaged image is optically subtracted continuously from the actual image. This operation is in fact an approximation of a temporal differentiation [14]. Thus, a photorefractive novelty filter is well suited for the visualization of continuous changes. We have illustrated this by realizing two exemplary applications, using for both cases our Co:$BaTiO_3$ crystal due to its potential to realize high contrast ratios in novelty filtering. In the experiments, the conditions for the optimization of the contrast derived in the previous chapter were used to adjust the devices to their best performance parameters.

3.1 Visualization of gas flows

The experimental setup for the visualization of gas flows is a straightforward extension of the simple two-wave-mixing setup shown in Fig. 2. The only difference is that the signal beam is expanded and focused into the crystal and the gas flow is made to pass the signal beam in the expanded region. As an example, we chose the gas flow out of a fire lighter, that was not lit. A series of snapshots showing the entrance of the gas into the observation region and its turbulent flow against an obstacle are shown in Fig. 6. Because the minimum speed that can be detected with the novelty filter is defined by the diffraction-limited smallest size d in the object divided by the characteristic photorefractive response time constant of the material [23], and is usually in the range of 1 μm/s, a broad range of gas flows can be visualized by this method. This clearly demonstrates the novelty filter's ability to detect continuous phase changes. Such phase changes may be of particular interest in different areas of science and technology as fluid dynamics, aerodynamics, and thermodynamics.

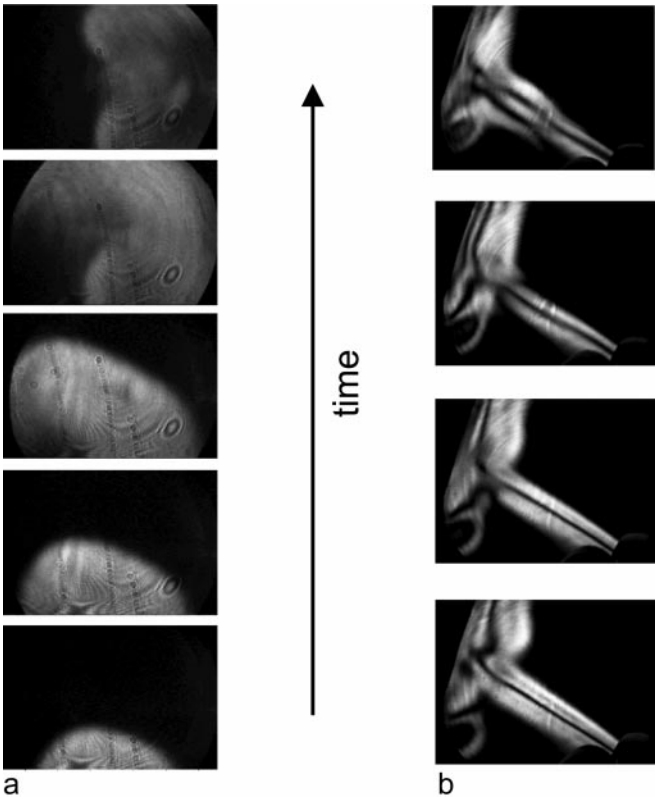

Fig. 6a,b. Time series of the gas flow from a fire lighter. (**a**) Entering the observation region. (**b**) In turbulent flowing against an obstacle in the *lower right corner*, visualized with the two-beam coupling novelty filter. Both image series cover a time period of 2 s

3.2 Motion-detecting microscopy

Another vivid example of the high application potential of optical novelty filters is the motion-detecting microscope, as first proposed and demonstrated by Cudney et al. [4]. The device consists of a two-beam-coupling novelty filter, in which the image information is imprinted on the image beam via a conventional microscopic setup. Thus, it enables us to observe only moving microscopic objects, while stationary ones remain invisible. The experimental setup we have used is depicted in Fig. 7. The image beam is expanded via a microscope objective, a pinhole and a lens to illuminate the microscopic objects, mounted via an object holder on an xy translational stage. Via a microscope objective and an ocular, the image was magnified, focused into the crystal and then filmed from a screen. The only difference from a conventional microscope is that no virtual image of the object is created, but a real image that is viewed on the screen. Using this setup, we have achieved an optical magnification of 200. An additional speckle suppression was achieved by a slight vibration of the screen via a loudspeaker, which leads to a time averaging of speckled images and thus to a reduction of the speckle contrast.

Using this setup, we have observed moving microorganisms in a drop of water. Due to a slight saturation of the camera detection, the contrast observed in the figures is smaller than the real experimental contrast in accordance with Fig. 4. In Fig. 8, a slipper animalcule with a size of approximately 70 μm is shown without novelty filtering (top) and with novelty filtering in two different moments in which it has made a sudden movement (bottom). It is interesting to note that, due to the sudden movement that is faster than the time constant of the novelty filter, the microscopic object appears in two positions in the novelty filtered image, which are the initial and the final position. Figure 9 shows an insect larva without novelty filtering (top), with novelty filtering at rest (middle), and with novelty filtering while it is suddenly bending its body. Again, the object is visible in two states in the

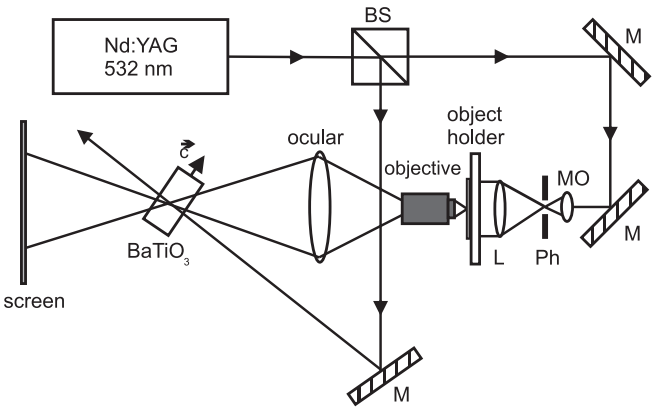

Fig. 7. Experimental setup of the motion detecting microscope. BS: beam splitter, M: mirrors, MO: microscope objective, Ph: pinhole, L: lens

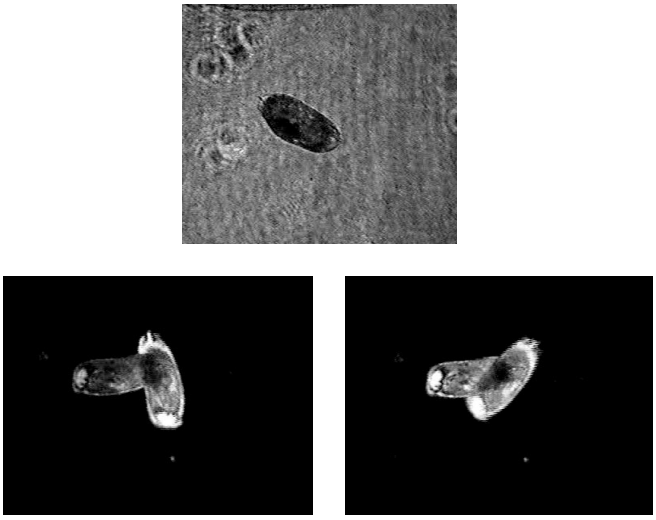

Fig. 8. Slipper animalcule (size approximately 70 μm), observed with the motion-detecting microscope. Top: without novelty filtering. Bottom: with novelty filtering, object at sudden motion

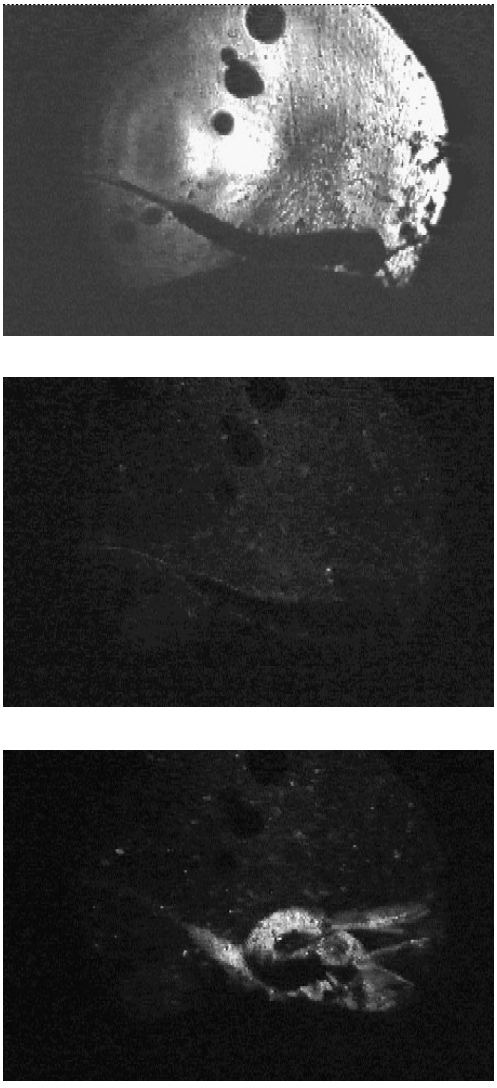

Fig. 9. Images of an insect larva. Top: without novelty filtering. Middle: with novelty filtering, but with object at rest. Bottom: with novelty filtering, object in sudden motion

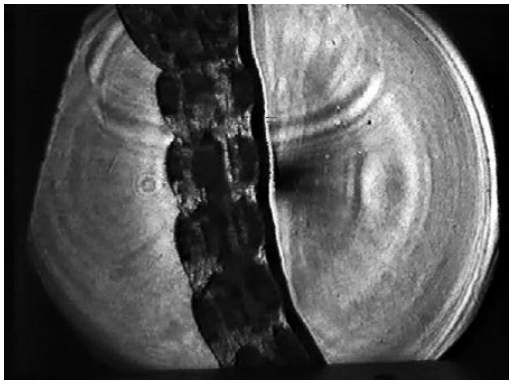

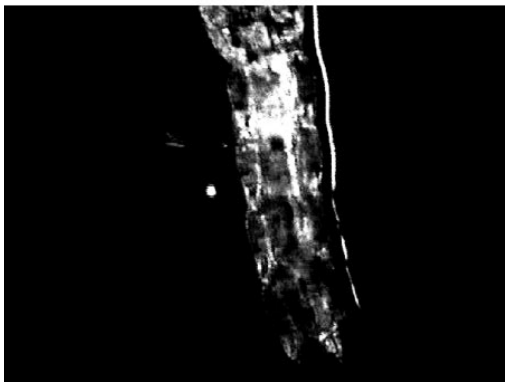

Fig. 10. Digestive system of a larger insect larva, observed with the motion-detecting microscope. Top: without novelty filtering. Bottom: with novelty filtering. The bright regions clearly indicate liquid flows

bottom image. We have also observed the digestive system of a larger insect larva using the motion detecting microscope. The results are shown in Fig. 10. The top image shows the object without novelty filtering and the bottom image with novelty filtering. It is important to note, that the object itself is at rest. Thus, the bright regions inside the objects are movements of liquids due to the larva's digestion.

4 Discrete changes: object comparison via image subtraction

Although a novelty filter performs a temporal differentiation of images with temporally continuous changes, it performs an image subtraction when the changes in the input image are temporally discrete. Thus, a novelty filter can be used as a parallel optical image subtractor. In contrast to electronic systems, the images do not have to pixelated.

For use in the field of object inspection, we have therefore realized a system that is capable of detecting the deviation of a test object from a given reference object. In our system, the image information of the objects is provided by the objects themselves, being placed in the image beam path, thus performing an amplitude modulation. Figure 11 shows the experimental setup used. The principle of operation of our method is as follows. The image beam is split by beam splitter 1 into a reference beam and an object beam, which are recombined via beam splitter 2 and are then incident on the crystal under the same angle. A liquid-crystal phase mod-

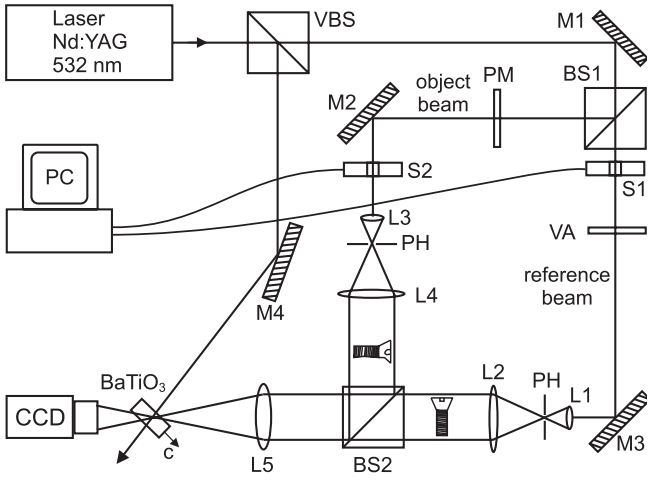

Fig. 11. Experimental setup for object comparison using the two-beam coupling novelty filter. VBS: variable beam splitter, BS: beam splitter L: lens, M: mirror, S: shutter, PH: pinhole, VA: variable attenuator, PM phase modulator

ulator PM is used to adjust the relative phases of the two beams. In order to achieve pure phase modulation, we constructed a single-field modulator filled with parallel nematic liquid crystals. The phase variation of this modulator could be adjusted by applying an external electric field from 0 to 3π with an accuracy better than 0.1π. During operation, the two image beams are switched alternately by electronically controlled shutters. Thus, no interference takes places in the beam splitter during the object inspection. First results of an object inspection using this method are shown in Fig. 12. Disturbances in this figure that result in a poorer object comparison result stem from inhomogeneities in the plane waves used in both arms.

In this configuration, we have reached an inspection rate of up to 4 Hz. This rate can be substantially enhanced if the image information of the test object is only incident for a short time period, just long enough to detect the result of the test. Under these circumstances, the hologram of the reference object stored in the crystal is not noticeably erased and the inspection rate is only limited by the time necessary to replace the test objects. The resolution of the system is in principle not limited by the inspection method itself but by the detection of the result via the CCD camera. The minimum resolvable object deviation appeared to be strongly dependent of the magnification of the result on the CCD chip via a lens system (not shown in Fig. 12). In our experiments, we were able to detect object deviations of down to 30 μm. Using CCD cameras with smaller pixel size, the minimum resolvable feature size could be further reduced. Due to the design of our setup including large aperture lenses, we were able to keep the average speckle size below the value of 30 μm. Thus, speckles are not limiting the resolution at the present status of the experiments. Attention should be paid to the fact that undesired relative transverse shifts of the objects are detected by the system in the same way as the deviations the system is wanted to detect. Thus, an automatic fine alignment of the test objects is desired. An extension of our system incorporating automatic object positioning based on optical correlation techniques is currently under investigation.

Fig. 12. Experimental result of object comparison. *Top*: master object. *Middle*: object under test. *Bottom*: detected output

5 Conclusion

We have first analyzed and optimized the performance of the two-beam coupling photorefractive novelty filter. Because the commonly accepted coupled-wave theory has proved to be incapable of describing the device's most important figure of merit, the novelty contrast, a simple but effective interference model was developed. This model is in good agreement with experimental measurements of amplitude contrast and phase contrast. The novelty filter was then applied to the visualization of temporally continuous changes in an image, namely a gas flow and micro-organisms. Its capability of performing an image subtraction for temporally discrete changes was exploited by the realization of an object inspection system based on image subtraction.

Acknowledgements. The authors acknowledge technical assistance by M. Fiegler. This work was partially supported by the Deutsche Forschungsgemeinschaft, Schwerpunkt "Automatische Sichtprüfung".

References

1. D.Z. Anderson, J. Feinberg: IEEE J. Quantum Electron. **QE-25**, 535 (1989)
2. D.T.H. Liu, L.-J. Cheng: Opt. Eng. **30**, 571 (1991)
3. M. Sedlatschek, T. Rauch, C. Denz, T. Tschudi: Opt. Commun. **116**, 25 (1995)
4. R.S. Cudney, R.M. Pierce, J. Feinberg: Nature **332**, 424 (1988)
5. J.E. Ford, Y. Fainman, S.H. Lee: Opt. Lett. **13**, 856 (1988)

6. P. Mathey, P. Jullien, A. Dazzi, B. Mazué: Opt. Commun. **129**, 301 (1996)
7. F.C. Jahoda, P.R. Forman, B.L. Mason: Opt. Lett. **16**, 1532 (1991)
8. C. Soutar, Z.Q. Wang, W.A. Gillespie, C.M. Cartwright: Optik **94**, 16 (1993)
9. Y. Zhang, R. Kachru: Appl. Opt. **35**, 6762 (1996)
10. H. Rehn, R. Kowarschik, K.H. Ringhofer: Appl. Opt. **34**, 4907 (1995)
11. M. Esselbach, A. Kiessling, H. Rehn, B. Fleck, R. Kowarschik: J. Opt. Soc. Am. B **14**, 846 (1997)
12. T. Suzuki, H. Fujiwara: Proc. SPIE **1319**, 87 (1990)
13. G. Zhou, L. Bintz, D.Z. Anderson: Appl. Opt. **31**, 1740 (1992)
14. M. Cronin-Golomb, A.M. Biernacki, C. Lin, H. Kong: Opt. Lett. **12**, 1029 (1987)
15. P. Yeh: *Introduction to Photorefractive Nonlinear Optics* (Wiley, New York 1993)
16. I. McMichael, P. Yeh: Opt. Lett. **12**, 48 (1987)
17. W.B. Lawler, C.J. Sherman, M.G. Moharam: J. Opt. Soc. Am. B **8**, 2190 (1991)
18. M. Born, E. Wolf: *Principles of Optics* (Pergamon, Oxford 1984)
19. P. Günter: Phys. Rep. **93**, 199 (1982)
20. N.V. Kukhtharev, V.B. Markov, S.G. Odoulov, M.S. Soskin, V.L. Vinetskii: Ferroelectrics **22**, 949 (1979)
21. F. Davidson, L. Boutsikaris, M. Krainak: Opt. Lett. **13**, 506 (1988)
22. M. Sedlatschek, T. Rauch, C. Denz, T. Tschudi: Opt. Mater. **4**, 376 (1995)
23. J. Khoury, G. Hussain, R.W. Eason: Opt. Commun. **71**, 138 (1989)